Carbohydrate Polymers 140 (2016) 374–382

Contents lists available at ScienceDirect

Carbohydrate Polymers

journal homepage: www.elsevier.com/locate/carbpol

Reinforcement effect of poly(butylene succinate) (PBS)-grafted cellulose nanocrystal on toughened PBS/polylactic acid blends

Xuzhen Zhang, Yong Zhang*

State Key Laboratory of Metal Matrix Composites, School of Chemistry and Chemical Engineering, Shanghai Jiao Tong University, 800 Dongchuan Road, Shanghai 200240, China

ARTICLE INFO

Article history:
Received 14 August 2015
Received in revised form 6 December 2015
Accepted 29 December 2015
Available online 31 December 2015

Keywords:
Cellulose nanocrystal
Poly(butylene succinate)
In situ polymerization
Dicumyl peroxide
Polylactic acid
Composite

ABSTRACT

Poly(butylene succinate) (PBS)/polylactic acid (PLA) blends modified with dicumyl peroxide (DCP) were reinforced by PBS-*g*-cellulose nanocrystal (CNC) through melt mixing. PBS-*g*-CNC was prepared through *in situ* polymerization and its structure was confirmed by FTIR, ^{13}C NMR, XPS and GPC analysis after saponification. The morphological analysis of PBS/PLA/PBS-*g*-CNC composites before and after etched by CH_2Cl_2 shows that the addition of DCP and PBS-*g*-CNC could decrease the size of PBS as a dispersed phase in PLA matrix and improve the dispersion of PBS-*g*-CNC in both PBS and PLA phases, which could affect the crystallization and mechanical properties of composites. The crystallinity of PLA α′-phase crystal in PBS/PLA/PBS-*g*-CNC composites is increased obviously by the addition of PBS-*g*-CNC, leading to an increase of the crystallinity of the composites. PBS/PLA blends modified by DCP have high Notched Izod impact strength and moduli, and the values are increased by the addition of PBS-*g*-CNC. Both storage modulus and glass translation temperature of PBS/PLA blend are increased by DCP and PBS-*g*-CNC, which is proved by DMA results, showing a weak molecular segment mobility of PBS/PLA matrix. The addition of DCP decreases the crystallization temperature and crystallinity of PBS/PLA composite, but increases the thermal stability of composites, mostly because of the crosslink effect of DCP on PBS/PLA matrix.

1. Introduction

Polylactic acid (PLA) is a bio-degradable polymer, and can be used as an environmental friendly plastic (Wang, Wang, Zhang, Wan, & Ma, 2009b). But the high production costs, brittle nature and slow crystallization rate of PLA restricts its applications as common polymers (Nerkar, Ramsay, Ramsay, Vasileiou, & Kontopoulou, 2015). Various modification methods have been employed to overcome these limitations of PLA (Anderson, Schreck, & Hillmyer, 2008; Rasal, Janorkar, & Hirt, 2010; Nagarajan, Zhang, Misra, & Mohanty, 2015). Modification of PLA by physical blending is a useful and economical way to improve the toughness. For example, some flexible biodegradable polymers such as poly(butylene succinate) (PBS) (Shibata, Inoue, & Miyoshi, 2006; Cherykhunthod, Seadan, & Suttiruengwong, 2015; Shibata, Teramoto, & Inoue, 2007), poly(butylene adipate-*co*-terephthalate) (PBAT) (Jiang, Wolcott, & Zhang, 2006) and poly(butylene succinate-*co*-adipate) (PBSA) have been used to toughen PLA. However, these blends prepared by simple melt blending could not achieve good mechanical properties due to the phase separation and poor interfacial adhesion between the two components.

As a crosslinking agent, dicumyl peroxide (DCP) was used to modify PLA/polyesters composites *via in situ* compatibilization (Zeng, Li, & Du, 2015). Ji et al. (2014) studied the effect of DCP on the morphology and properties of PLA/PBS composites, and found that the interfacial adhesion between PLA and PBS was increased significantly as evidenced by the decreased PBS particle size with increasing DCP content, which resulted in significant improvement in mechanical properties. Similarly, DCP was also used to improve the interfacial adhesion between PLA and PBAT (Signori et al., 2015; Ma et al., 2014). The addition of DCP could decrease the PBAT phase size and led to the formation of PBAT gel which had a toughing effect on PLA. However, PLA/polyesters blends still have poorer thermal stability and mechanical properties especially lower impact strength than those commodity plastics such as polypropylene.

Cellulose nanocrystal (CNC) may be a good choice to reinforce PLA-based composites, because it is a promising biopolymer filler used to reinforce many bio-based polyesters, such as PLA (Lizundia, Vilas, & León, 2015), PBS (Lin, Yu, Chang, Li, & Huang, 2011b), PBSA (Zhang & Zhang, 2015) and PBAT (Ludvik, Glenn, Klamczynski, & Wood, 2007) with appealing intrinsic properties such as good mechanical properties (longitudinal modulus

* Corresponding author. Tel.: +86 21 54743257; fax: +86 21 54741297.
E-mail address: yong_zhang@sjtu.edu.cn (Y. Zhang).

http://dx.doi.org/10.1016/j.carbpol.2015.12.073
0144-8617/

close to 150 GPa), high aspect ratio (10–70) and high surface area (Kargarzadeh, Sheltami, Ahmad, Abdullah, & Dufresne, 2015; Arrieta, Fortunati, Dominici, López, & Kenny, 2015). To improve the dispersion of CNC and its adhesion to polymers, some CNC surface modification methods, such as acetylation (Lin, Huang, Chang, Feng, & Yu, 2011a), and reactions with castor oil (Shang et al., 2013), waterborne epoxy (Xu, Girouard, Schueneman, Shofner, & Meredith, 2013) and polyurethane (Rueda et al., 2013). All the methods could successfully improve the dispersion of CNC in bio-based polymers, but the improvement in their adhesion was still limited, which is partially because of the limited compatibility of those modifiers with the polymer matrices. On this occasion, *in situ* polymerization method was used to prepare polymer grafted CNC composites, and to improve the compatibility of CNC and polymeric matrix. Cao, Habibi, and Lucia (2009) prepared waterborne polyurethane/CNC composites successfully *via in situ* polymerization, and observed that a co-continuous phase between the matrix and CNC was formed which enhanced the interfacial adhesion and consequently contributed to an improvement in the thermal stability and mechanical strength of the composites.

In this study, poly(butylenes succinate)-grafted cellulose nanocrystal (PBS-*g*-CNC) was prepared through *in situ* polymerization. PBS-*g*-CNC was then used to reinforce DCP modified PBS/PLA composites in order to have a good dispersion and compatibility with PBS component. The structure of PBS-*g*-CNC was characterized with FTIR, ^{13}C NMR, XPS as well as gel permeation chromatography (GPC) and the morphology of composites was observed by scanning electron microscope. The effects of PBS-*g*-CNC and DCP on the compatibility of PBS and PLA were studied. The crystallization behavior, mechanical properties and thermal stability of the composites were also investigated.

2. Experimental

2.1. Materials

PLA (Revode 190) with number average molecular weight (M_n) of 9.7×10^4 g/mol, polydispersity index (PDI) of 1.2, and L-lactate unit content of 98.5% was kindly supplied by Zhejiang Hisun Biomaterials Co., Ltd. (China). PBS (Bionolle 1001MD) was produced by Showa Denko Group (Japan) with M_n of 8.8×10^4 g/mol and PDI of 2.2. DCP, 1,4-butanediol (BDO), succinic acid (SA) and microcrystalline cellulose (MCC) were purchased from Sinopharm Chemical Reagent Co., Ltd. (China). Titanium butoxide (97%), purchased from Sigma-Aldrich (USA), was used as a catalyst. CNC with length of 100–250 nm and diameter of 15–30 nm was extracted from MCC in sulfuric acid solution with a similar method used in the study of Lin et al. (2013).

2.2. Synthesis of PBS-g-CNC via in situ polymerization

Synthesis of PBS-*g*-CNC consisted of two steps: the esterification of BDO, CNC and SA to obtain an oligomer, and the synthesis of high-molecular weight PBS-*g*-CNC by condensation polymerization.

CNC, BDO and SA were added into a four-necked flask with a weight ratio of 20:33:67, and heated to 180 °C until SA was completely dissolved in BDO under N_2 atmosphere. When no more water was distilled out under normal pressure, titanium butoxide (0.1% of total amount of the reactants) as a catalyst was added into the flask and the reaction system was heated to 220 °C under high vacuum and kept for 4 h to obtain a mixture of *in situ* condensation polymerization.

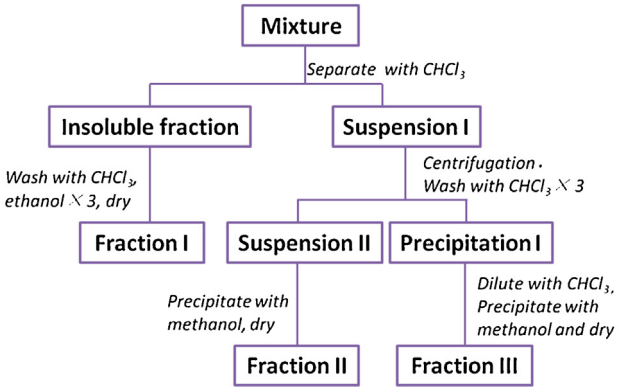

Scheme 1. Extraction and separation procedure of the PBS-*g*-CNC copolymer.

2.3. Extraction of PBS-g-CNC

The mixture was added in chloroform and stirred for 24 h at room temperature to form a suspension (noted as Suspension I) and an insoluable fraction floating on the surface of the suspension. The insoluable fraction was washed by chloroform and ethanol for 3 times, respectively. To remove PBS homopolymer and residual reactants, and the residue was vacuum-dried at 60 °C for 6 h and named as Fraction I.

To remove PBS homopolymer, Suspension I was subjected to 3 times of centrifugation at 10,000 rpm for 30 min to get a suspension (Suspension II) and precipitation (Precipitation I). After each centrifugation, the precipitate in suspension was separated and diluted again in chloroform. 5 min ultrasonic treatment was necessary to obtain a uniform suspension before next centrifugation. Suspension II was deposited in methanol and vacuum-dried to obtain Fraction II (possibly PBS). Precipitation I was first dispersed in chloroform to get a suspension, and then precipitated by methanol and vacuum-dried at 60 °C for 24 h to get Fraction III (PBS-*g*-CNC). The procedure details of separation are presented in Scheme 1. In order to control the veracity of the following tests, Fraction III was subjected to Soxhlet extraction with chloroform for 24 h.

To investigate the PBS molecular structure connected onto the surface of CNC, PBS-*g*-CNC composite was subjected to a saponification in order to cleave the PBS chains from CNC. 1 g PBS-*g*-CNC composite was dispersed in 50 mL sodium hydroxide solution with a sodium hydroxide concentration of 0.5 mol/L, and the saponification was started at 30 °C with magnetic stirring. Samples were taken out every 5 min, and the PBS component in each sample was then separated from CNC by suction filtration and Soxhlet extraction for gel permeation chromatography test using chloroform as solvent. The bore diameter of Teflon filter paper used in suction filtration was 200 nm.

2.4. Preparation of PBS/PLA/DCP/(PBS-g-CNC) composites via melt blending

PBS and PLA were first vacuum-dried for 12 h at 80 °C. PBS/PLA(30/70) blend was prepared using a Haake rheometer at a rotor speed of 60 rpm and 190 °C for 10 min, and compression molded for 10 min at 200 °C to get sheets with the thickness of 1 and 3 mm for measurements. For PBS/PLA/DCP/(PBS-*g*-CNC) composites, DCP/(PBS-*g*-CNC) ratio was as follows: 0/0, 0/2, 0.2/0, 0.2/0.5, 0.2/1.0, 0.2/2.0.

2.5. Characterization

Infrared spectra were obtained by using a Spectrum 100 Fourier transform infrared spectra (FTIR) Spectrometer (Perkin Elmer,

USA). Solid-state ^{13}C spectra were obtained with a Avance III 600 NMR spectrometer (Bruker, Germany) at 100 MHz under cross-polarization while spinning at the magic angle. Power decoupling conditions were set with a 90° pulse and 4-s cycle time. X-ray photoelectron spectroscopy (XPS) measurements were performed on an AXIS Ultra DLD (Kratos, Japan) spectrometer at room temperature with a base pressure of 1×10^{-9} Mbar. Quantitative XPS analysis was performed with the Kratos Vision Software. The level of modification on CNC was determined by elemental analysis using a Vario EL Cube elemental analyzer (Elementar, Germany). The number-average molecular weight (M_n) and its distribution (PDI, M_w/M_n) for PBS cleaved from PBS-*g*-CNC composite were tested by GPC (Waters, USA) at 30 °C with a calibration curve constructed using polystyrene standards. Chloroform was used as a solvent with a flow rate of 1.0 mL/min. Blend samples were cryogenically fractured in liquid nitrogen, and their fracture surfaces were etched by immersing in CH_2Cl_2 at 5 °C for 40 s to move PLA from PBS/PBS, and observed using scanning electron microscopy (SEM, FEI Co., USA). WAXD diffraction experiments were performed on a D/max-200/PC X-ray generator (Rigaku Cor., Japan) operated at 40 kV and 20 mA with Cu-*K*α radiation (λ = 0.154 nm) at a scanning rate of 4°/min, and a Jade software was used to deduct the amorphous peak of PBS and analyze crystal peaks according to the method of Guo et al. (2012).

Tensile and Flexural properties were measured using a universal test machine (SANS, MTS Systems Cor., USA). Tensile properties was tested at a crosshead speed of 20 mm min^{-1}, following ASTM D882-10. Dumbbell samples were prepared by cutting composites sheets into 75 mm in length, 1 mm in thickness, and 4 mm in width. Notched Izod impact strength was tested using a Ray-Ran universal Pendulum Impact Tester according to ASTM D256. The dimension of the samples for impact and flexural testing was $63.5 \times 12.7 \times 3$ mm^3. All samples were kept at 23 °C, 50% humidity for 24 h before testing.

Dynamic mechanical analysis (DMA) was performed on a DMA 8000 dynamic mechanical analyzer (Perkin Elmer Co., USA) with a dual cantilever device at a frequency of 3 Hz. The temperature range was from −150 to 120 °C with a heating rate of 3 °C/min. Glass transition temperature and melting behavior were characterized by using a DSC (Q2000, TA Instruments) at 20 °C/min in nitrogen. A sample was heated from −50 to 200 °C to eliminate previous thermal history, then cooled down to −50 °C, and finally heated to 200 °C. Thermal stability was characterized by using a thermogravimetric analyzer (Q5000, TA Instruments, USA). A sample was heated from 40 to 600 °C at a rate of 20 °C/min under nitrogen atmosphere.

3. Results and discussion

3.1. Structure analysis of PBS-g-CNC

FTIR spectra of Fractions I–III are shown in Fig. 1(a). Compared with CNC, Fraction I has the same peaks except for a weak peak around 1726 cm^{-1}, which is related to the C—O bond in ester group of PBS (Lin et al., 2011a). Therefore, the main composition of Fraction I is CNC, and there is a small amount of PBS component. Fraction II and PBS have similar FTIR spectra, indicating Fraction II is basically PBS. The absorption peaks of Fraction III are nearly the same as that of Fraction II except for a stronger and wider peak around 3432–3343 cm^{-1} in Fraction III. The peaks at 3432 cm^{-1} and 3343 cm^{-1} can be attributed to —OH group of free water or the pyranose rings of CNC (Lin & Dufresne, 2013). Even though water can be rarely removed completely from a cellulose surface, these peaks should be mostly contributed by –OH on the pyranose rings of CNC considering all fractions are dried under the same condition and there should be a little free water. As a result, Fraction III could be confirmed as PBS-*g*-CNC. Further evidence of esterification between PBS and CNC was provided by solid-state ^{13}C NMR spectroscopy, as shown in Fig. 1(b). The ^{13}C NMR spectrum of PBS exhibits peaks at δ of 64.2, 25.0, 172.1 and 28.9 ppm (Zheng, Li, Zhang, Guan, Xiao, & Wang, 2011). Compared with that of PBS, the spectrum of PBS-*g*-CNC contains three additional peaks at δ of 62.0, 68–75 and 97.5 ppm, which are contributed by CNC component. The grafting reaction of PBS onto CNC can be confirmed by the presence of the three peaks, which matches the results of FTIR results.

XPS spectra are determined for the main elements and the carbon-based bonds in order to evaluate the chemical composition, especially the occurrence of PBS before and after grafting reaction. The low resolution spectra of CNC, PBS and PBS-*g*-CNC show that carbon and oxygen atoms are the main components. While in the high resolution carbon spectra (inside Fig. 2), the carbon signal can be resolved into several component peaks, which reflect the local environments of the carbon atoms (C—C and C—H, C—O, O—C—O, or O—C═O). In PBS-*g*-CNC (Fraction III) spectrum, the peaks of the four kinds of carbon atoms are categorized by the kind of bonds whether carbon atom is involved in PBS and/or CNC. The relative amount of each carbon type in the samples is determined by calculating the area of peaks and the results are summarized in Table 1. The ratio of carbon atoms with two bonds to oxygen relative to carbon atoms with one bond to oxygen (O—C—O/C—O) is found to be 0.198 which is very close to the theoretical value of 0.2 expected from the formula of CNC $(C_6O_5H_{10})_n$. After the *in situ* polymerization, the proportion of each carbon atom significantly varied, which is especially true for the proportions of C—C and O—C═O. The presence of PBS macromolecules on the surface could be used to explain the high proportions of these types of carbon atoms. These results further confirm the presence of PBS grafted on CNC.

Results for elemental analyses of CNC, PBS and PBS-*g*-CNC are presented in Table 1. The ratio of carbon atoms to oxygen atoms is found to be 1.65 and 0.83 for PBS and CNC, which are close to the theoretical value of 1.5 and 0.8 expected from their formulas, respectively. According to the proportions of O and C, the content of PBS grafted on CNC is calculated to be 6.07/7.07 (based on PBS-*g*-CNC content).

The effect of saponification time on M_n and PDI of PBS macromolecules dissociated from PBS-*g*-CNC is shown in Table 2. The initial M_n is about 2.37×10^4 with a high value of PDI, and M_n decreases slowly with saponification time in the first 5 min. This indicates that M_n of PBS chains grafted on CNC is 2.37×10^4 or higher, and the corresponding degree of polymerization is 140 or higher. M_n reaches the lowest value of 0.23×10^4 at saponification time of 25 min, and this decrease in M_n with low PDI is a consequence of both the further dissociation of PBS macromolecules and the hydrolysis of PBS macromolecules dissociated from PBS-*g*-CNC.

3.2. Fracture morphologies of composites

The phase morphology should be a key factor affecting the properties of PBS/PLA blend. As a thermodynamically incompatible system, the melt blended PBS/PLA blends normally present a typical two-phase structure incorporated with microsized PBS particles (Wu, Yuan, Laredo, Zhang, & Zhou, 2012). The large size of dispersed phase is a main challenge for good mechanical properties of PBS/PLA composites. Fig. 3 reveals the phase morphology of the PLA/PBS composites by direct SEM observation and quantitative size analyses after etching the PLA matrix of composites. The classic “sea-island” structure and poor interaction, in which discrete droplets of PBS phase are dispersed in PLA phase with obvious interfacial bonding, is evidently presented in the PBS/PLA composites as shown in Fig. 3(a1–a4). It essentially arises from the thermodynamic incompatibility (Zhang, Mohanty, & Misra, 2012)

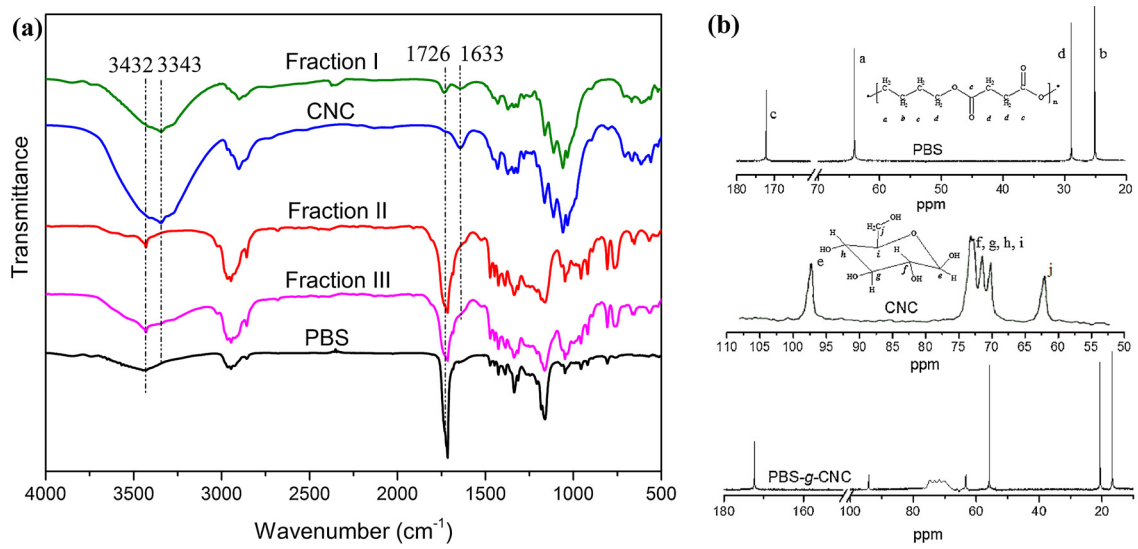

Fig. 1. (a) FTIR spectra of neat PBS, CNC, extracted fractions and (b) ^{13}C NMR spectra of PBS, CNC and PBS-*g*-CNC.

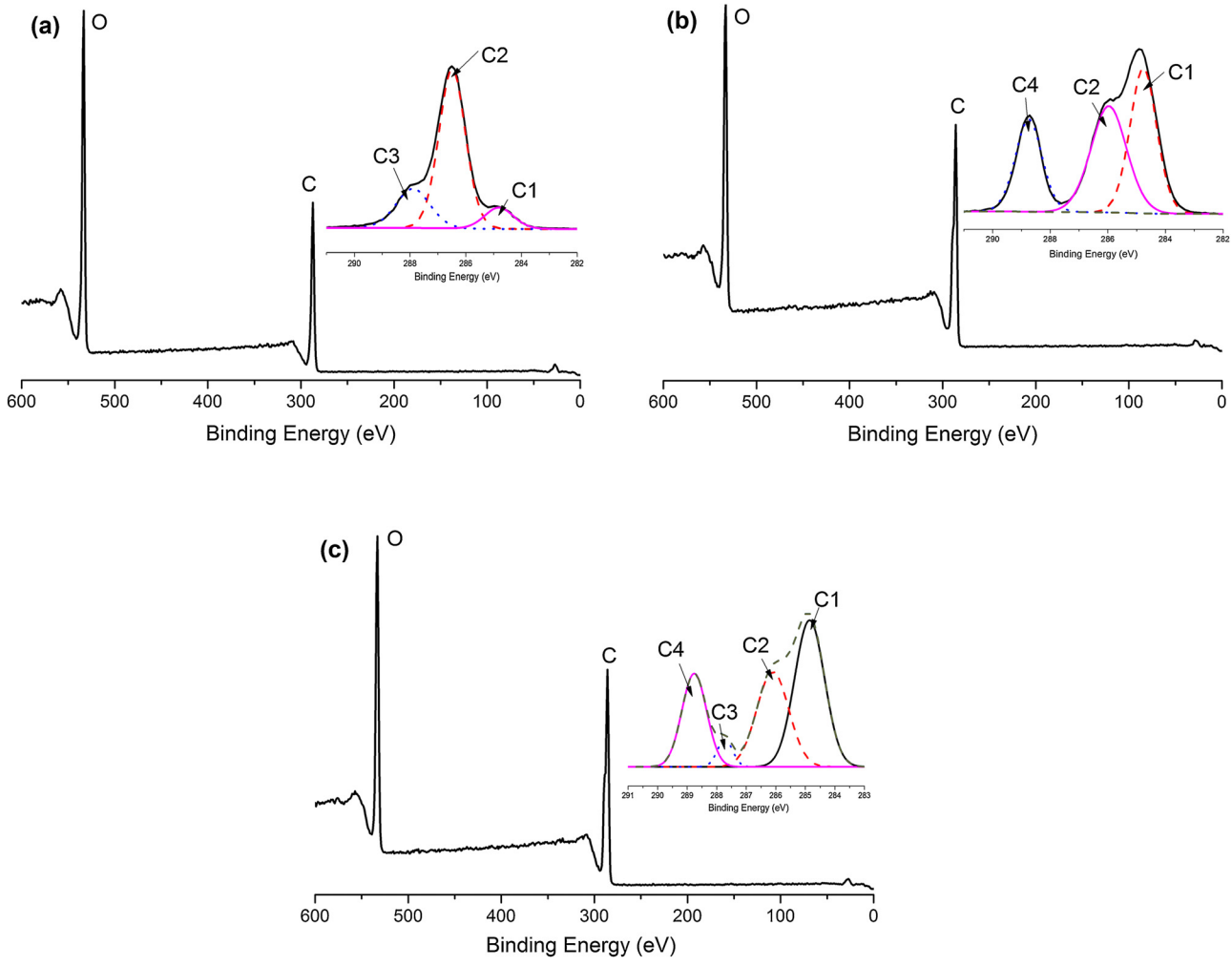

Fig. 2. XPS wide scans from CNC (a), PBS (b) and PBS-*g*-CNC (c). Insets: high resolution carbon spectura: C1: C—C, 285.0 eV; C2: C—O, 286.5 eV; C3: O—C—O, 288.0 eV; C4: O—C=O, 289.0 eV.

and high interfacial tension (~3.7 mN/m) (Xu & Huang, 2012) between PBS and PLA. Fig. 3(a2–d2) clearly demonstrates the presence of PBS droplets by etching PLA component, yielding the quantitative analyses regarding the distribution of the droplet size as shown in Fig. 3(a4–d4). The average area (A) of PBS droplets decreases from 9.11 μm^2 to 3.89 and 4.66 μm^2 after adding 0.2 phr DCP and 2 phr PBS-*g*-CNC into PBS/PLA composites, respectively. After introducing DCP into the PBS/PLA matrix along with

Table 1
Elemental composition (%) for PBS, CNC and PBS-*g*-CNC composite.

Sample	O[a]	H[a]	C[a]	C1[b]	C2[b]	C3[b]	C4[b]
PBS	35.6	7.15	58.7	45.1	31.3	NA	23.6
CNC	51.3	6.0	42.7	17.1	69.2	13.7	NA
PBS-*g*-CNC	38.6	6.93	57.6	42.9	30.8	3.8	22.5

[a] Estimated by mass difference.
[b] From area of corresponding peaks in Fig. 2. NA—not analysable by the method employed.

Table 2
M_n and PDI of PBS chain dissociated from PBS-*g*-CNC composite *versus* saponification time (min).

Time (min)	1	2	4	6	10	15	20	25	30
M_n ($\times 10^4$)	2.37	2.36	2.31	2.26	1.85	1.26	0.62	0.32	0.23
PDI	2.54	2.63	2.74	1.93	2.32	2.06	1.95	1.68	1.26

PBS-*g*-CNC, the average area of PBS droplets is decreased to 1.53 μm^2, which is much lower than the common PBS/PLA systems (Nerkar et al., 2015), accompanied by the significantly deceased area distribution width as shown in Fig. 3(d1–d4). The decrease of PBS droplet average area implies that both DCP and PBS-*g*-CNC could improve the compatibility of PBS and PLA, and a synergy effect between DCP and PBS-*g*-CNC.

After added into PBS/PLA matrix, PBS-*g*-CNC was dispersed in both PBS and PLA phases, as shown in Fig. 3(c3 and d3), which should contributes to enhancement of both PBS and PLA phases, and consequently affect the mechanical properties and crystallization behavior of composites and avoid stress concentration when the composites are applied to external force.

3.3. Crystalline properties

The WAXD patterns of PBS/PLA composites were investigated to obtain insight into crystallinity, as shown in Fig. 4. A broad diffraction peak accompanied with two weak peaks was observed for PLA, indicating that the specimen at the processing condition is mostly amorphous with very low crystallinity. The peaks locating at 16.5° and 18.8° are contributed from (2 0 0)/(1 1 0), (2 0 3) planes of α′-phase crystal in PLA (Kawai et al., 2007; Yasuniwa, Sakamo, Ono, & Kawahara, 2008). The crystal unit cell of PBS is monoclinic and the diffraction peaks from (0 2 0), (0 2 1) and (1 1 0) are observed at Bragg angles of 19.5°, 21.5° and 22.5°, respectively (Ahn, Kim, Kim, & Yang, 2001). After adding 2.0 phr PBS-*g*-CNC or 0.2 phr DCP, PBS/PLA composites show stronger peak at 16.5°, indicating both DCP and PBS-*g*-CNC can contribute to the growth of α′-crystal of PLA. When the DCP content is 0.2 phr, the peak height of α′-crystal, locating at 16.5° and 18.5°, is increased with increasing PBS-*g*-CNC content while the peak height corresponding to PBS crystal has little change. As a result, the crystallinity of composites, *i.e.*, the summation of crystallinities of PBS and PLA components in each composite, increased from 12% to 30% with increasing PBS-*g*-CNC content from

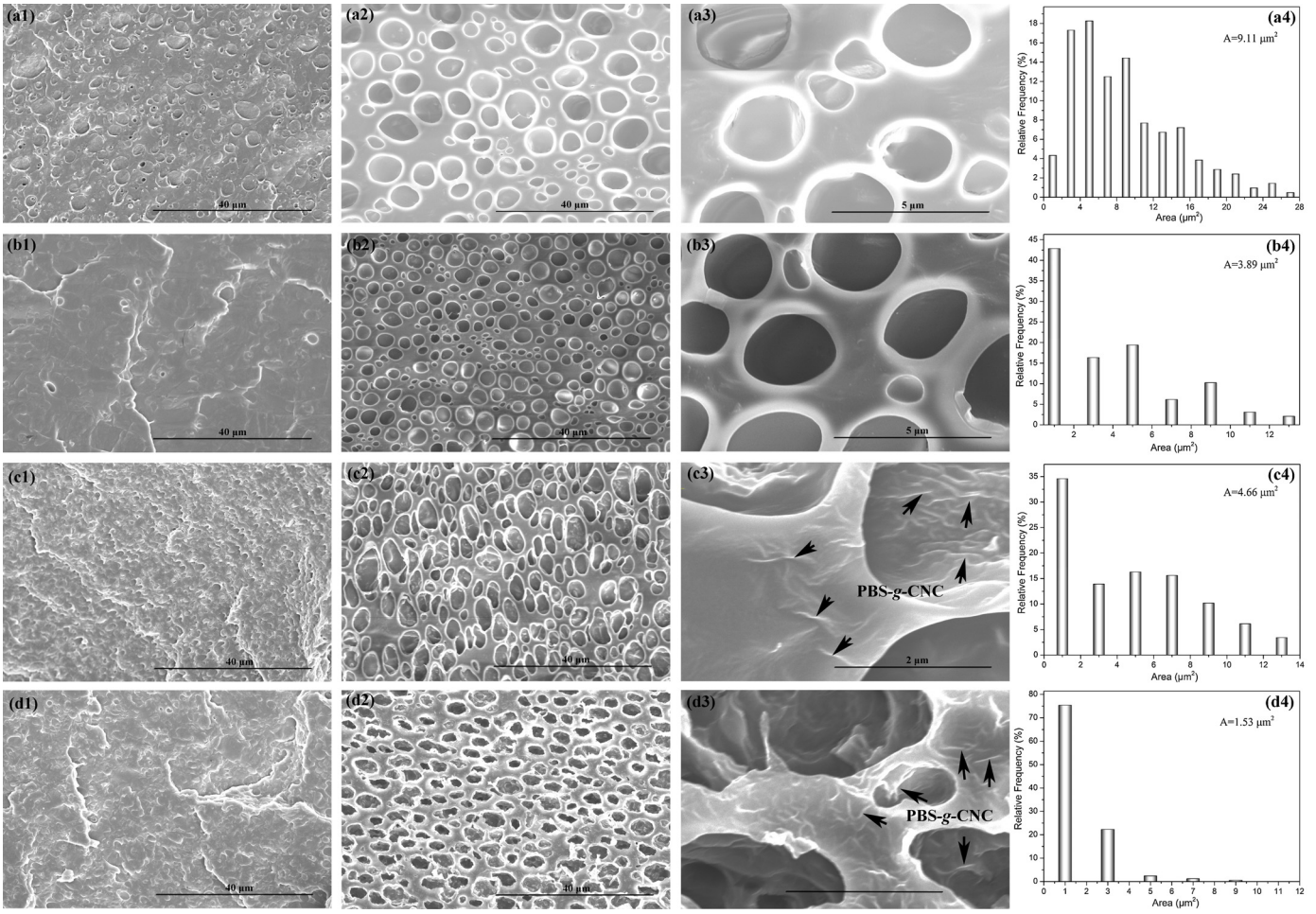

Fig. 3. SEM images of cryogenically fractured surface of composites with PBS/PLA/DCP/(PBS-*g*-CNC) ratio of (a1) (30/70/0/0), (b1) (30/70/0.2/0), (c1) (30/70/0/2) and (d1) (30/70/0.2/2). (a2)–(d2) present the dispersed-phase morphology of PBS and CNC after etching the PLA matrix of (a1)–(d1), which produce the quantitative analyses in terms of the distribution of PBS phase size as shown in (a4)–(d4), respectively. The higher resolution version of (a2)–(d2) are exhibited in (a3)–(d3). The average area (A) is marked in the right up corner of (a4), (b4), (c4) and (d4).

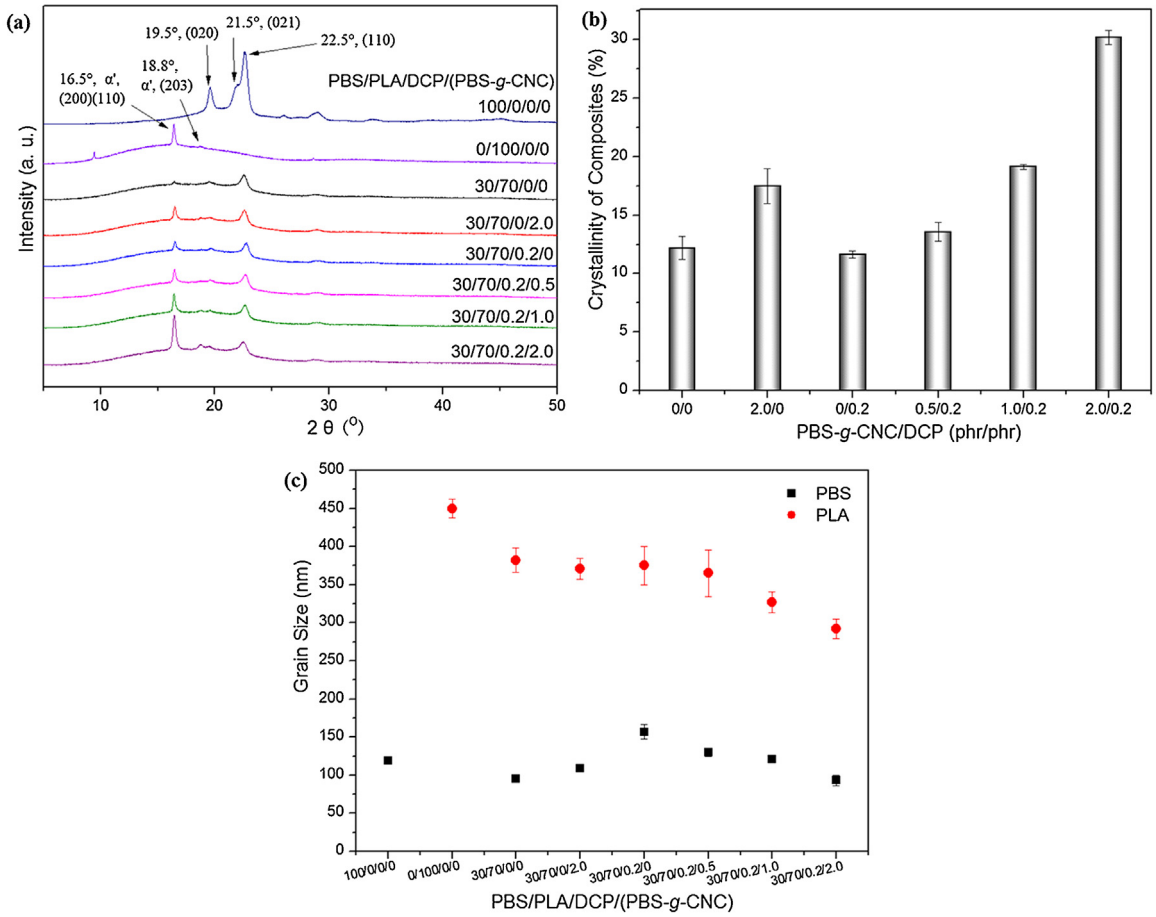

Fig. 4. (a) WAXD patterns, (b) the crystallinity histogram, and (c) crystal sizes of PBS/PLA based composites.

0 to 2.0 phr (image b). That is evidence that the addition of PBS-*g*-CNC into PBS/PLA can increase the crystallinity of PLA component in PBS/PLA composites. The addition of 0.5 phr PBS-*g*-CNC into PBS/PLA increases the crystal size of PLA crystal, but slightly affects the crystal size of PLA crystal. With further increasing PBS-*g*-CNC, the crystal size of both PLA and PBS crystals decreases. It can be concluded that the addition of PBS-*g*-CNC can increase the crystallinity of PBS/PLA and affect the crystal size of both PLA and PBS crystals.

3.4. Mechanical properties

PLA is known as a brittle polymer with a high tensile strength (69 MPa), low impact strength (105 MPa) and low elongation at break (4%) (Wang, Wang, & Zhang, 2009a). As shown in Table 3, the ductility of PLA significantly increased with the incorporation of 30% PBS, which is evidenced by the increases in the elongation and impact strength.

The impact strength evaluation is an important tool to study the fracture toughness of polymer composites. Table 3 also compares the impact strength of PBS/PLA blend with its composites. The Notched Izod impact strength and modulus of the PBS/PLA composite are significantly affected by DCP and PBS-*g*-CNC. With increasing PBS-*g*-CNC content from 0 to 2.0 phr, the impact strength of PBS/PLA with 0.2 phr DCP increases from 105 to 726 J/m, and this increasing extent is much higher than that of PBS/PLA composites in other researches (Harada et al., 2007). During drawing process, all samples exhibit typical ductile fracture behavior, and the values of tensile stress reach the maximum at the yield stain of 6.51–8.79%. The yield stress of PBS/PLA increases gradually with increasing PBS-*g*-CNC content. In addition, both flexural and Young's modulus are increased by the addition of PBS-*g*-CNC but slightly decreased after adding DCP. When the DCP content is 0.2 phr and the PBS-*g*-CNC content is 1.0 phr or higher, the PBS/PLA composites have higher moduli than the PBS/PLA blend. The decrease of modulus after the addition of DCP is reasonable because DCP can lead to some gels in polymer matrix due to the crosslinking effect, which will decrease the modulus of composites. The increased crystallinity by the addition of PBS-*g*-CNC in α′-phase crystal of PLA certified in WAXD pattern and the original high modulus of CNC should be the two main reasons for the increase in composites modulus.

3.5. Dynamic mechanical properties

Fig. 5(a) shows the storage modulus curves of PBS /PLA composites. The storage modulus (E') of PBS/PLA blend at room temperature is about 1.7 GPa, a little lower than that of composites with 0.2 phr DCP or 2.0 phr PBS-*g*-CNC. PBS-*g*-CNC is more effective than DCP when used as an impact modifier for PBS/PLA, implying an enhanced interfacial adhesion between PBS-*g*-CNC and PBS/PLA matrix. PBS/PLA/DCP/PBS-*g*-CNC (30/70/0.2/2.0) composite shows highest storage modulus at a given temperature under 48 °C. With increasing temperature over the glass transition temperature (T_g) of PLA, the storage modulus of composites decreases sharply due to the occurrence of glass transition.

As shown in Fig. 5(b), a sharp tan δ peak is observed around 55 °C for PBS/PLA blend, corresponding to the glass transition temperature of PLA. An obvious shift in tan δ peak toward higher

Table 3
Mechanical properties of PBS/PLA (30/70) composites.

Samples DCP/PBS-*g*-CNC	Notched Izod impact strength (J/m)	Flexural strength (MPa)	Yield stress (MPa)	Yield strain (%)	Stress at break (MPa)	Elongation at break (%)	Flexural modulus (GPa)	Young's modulus (MPa)
0/0	52	61.8	44.5	6.51	32.7	277	1.50	22.1
0/2.0	325	62.9	45.1	7.56	31.1	266	1.52	34.3
0.2/0	105	62.9	46.5	5.67	30.9	293	1.45	19.8
0.2/0.5	266	63.8	46.9	8.79	32.6	286	1.48	19.6
0.2/1.0	478	64.0	50.0	6.86	44.4	282	1.62	24.7
0.2/2.0	726	69.1	48.5	7.60	43.3	298	1.73	27.9

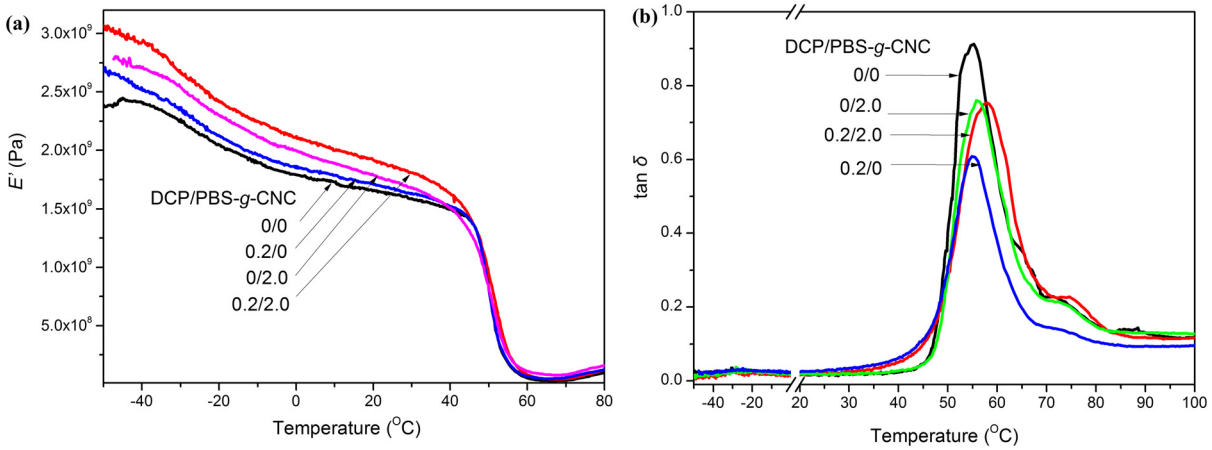

Fig. 5. DMA traces of PBS/PLA (30/70) composites with DCP and PBS-*g*-CNC: (a) storage modulus *versus* temperature; (b) tan δ *versus* temperature.

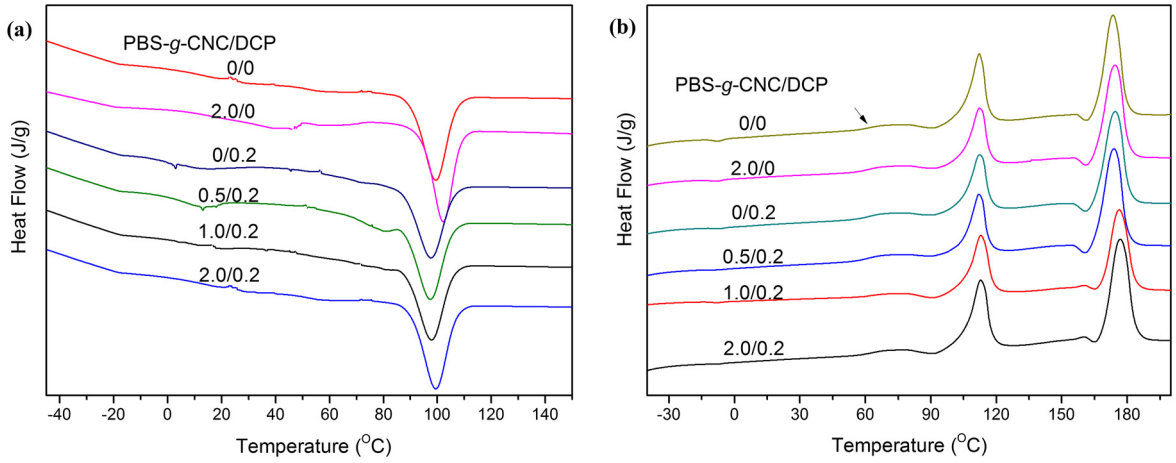

Fig. 6. DSC thermograms of PBS/PLA (30/70) composites on (a) cooling run and (b) 2nd heating run at a rate of 20 °C/min.

temperatures can be observed for the composite with 2.0 phr PBS-*g*-CNC, which indicates 2.0 phr PBS-*g*-CNC plays good reinforcement filler for PLA/PBS and hinders the movement of macromolecular segments. The addition of DCP has little effect of on the shift of tan δ peak, and this phenomenon is similar to the results of other researchers (Wang et al., 2009a) and is mostly because of the very low content of DCP in composites. In Fig. 5(b), it is very hard to observe the tan δ peak contributed by PBS segments in the temperature range of −40 to −10 °C, which may be related to the high crystallinity of PBS phase.

3.6. Thermal properties

Both PBS and PLA are typical semicrystalline polymers. Their mechanical and thermal resistance properties are greatly

Table 4
Thermal properties of PLA/PBS (30/70) composites modified with PBS-*g*-CNC and DCP.

DCP/PBS-*g*-CNC	T_{mc} (°C)	T_m (°C)		ΔH_m (J/g)		X (%)	
		PBS	PLA	PBS	PLA	PBS	PLA
0/0	102	113	177	20.4	29.5	34.0	46.0
0/2.0	102	113	176	22.8	28.2	38.0	46.8
0.2/0	97	112	174	15.6	30.0	26.0	44.0
0.2/0.5	98	112	174	17.1	31.3	28.5	48.8
0.2/1.0	98	112	174	17.1	31.3	28.5	48.8
0.2/2.0	100	112	173	19.2	28.7	32.0	49.8

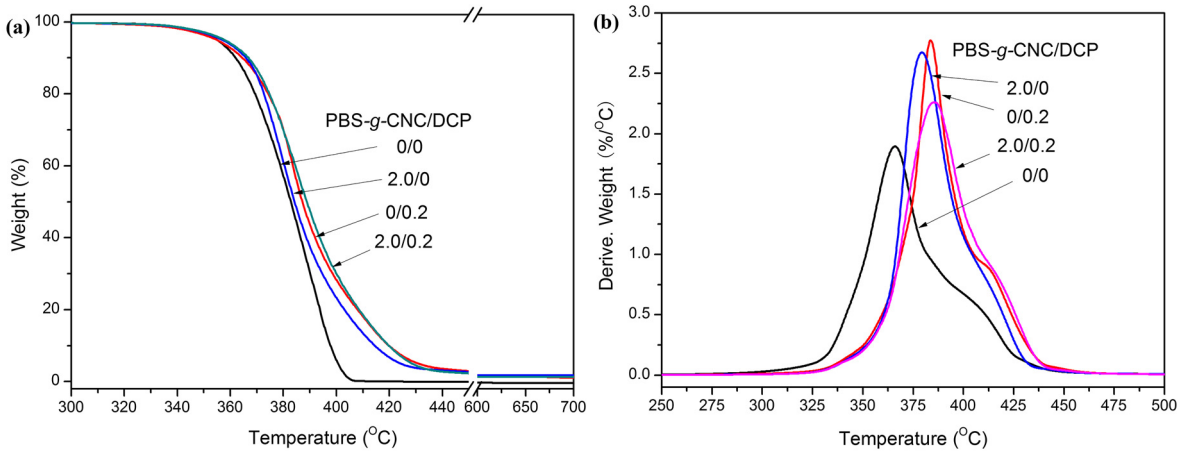

Fig. 7. TGA and DTG curves of PBS/PLA(30/70) blend.

dependent on the solid-state morphology and crystallinity. Accordingly, it is very importance to study the influence of the other minor components on the crystallization of matrix polymers in the blend. Fig. 6 shows the cooling and the second heating run thermograms of PBS/PLA, and the corresponding data are summarized in Table 4. In Fig. 6(a), only one exothermic peak located around 100 °C can be observed in all composites curves, and similar results are also reported by other researchers (Zhang et al., 2012). The crystallization temperature (T_{mc}) of PBS/PLA composites is decreased to a lower temperature with the addition of 0.2 phr DCP, indicating that the crystallization of PBS/PLA is restricted by the presence of DCP. Such results can be explained by the reason that the presence of DCP has a crosslink effect on PBS/PLA, restricting the movement of molecular segments and making it very difficult to complete the crystallization.

In Fig. 6(b), no obvious change can be observed for the T_g of PLA in the composites compared to that of PBS/PLA blend, which is different from the results of WAXD. The melting peaks corresponding to PBS and PLA components are obviously separated in the curves around 110 and 175 °C, respectively. The melting points of both PBS and PLA have little change after modification, but their melting enthalpy changes a lot. The crystallinity of PBS and PLA components is calculated according to the melting enthalpy and their content in composites as listed in Table 4. PBS/PLA shows a crystallinity of 34% for PBS component and 46% for PLA component, respectively. The crystallinity changes of both PBS and PLA are similar after adding 0.2 phr DCP, the values are decreased to 26 and 44%, respectively. This may be ascribed to low molecular segment mobility during crystallization. The segment mobility is a major factor for the crystallization ability of both PLA and PBS. However, compared with DCP, PBS-*g*-CNC is more efficient in promoting the crystallization of PBS and PLA. The crystallinity of PBS/PLA is slightly increased when adding PBS-*g*-CNC separately. When the DCP content is 0.2 phr, the crystallinity of PBS/PLA is also slightly increased with increasing PBS-*g*-CNC content. These results are similar to that of crystallinity in WAXD discussed above. And the increased crystallinity of composites should have contributed to the modulus of composites while maintaining the flexural toughness effect of DCP.

Fig. 7 shows the TGA curves of PBS/PLA composites. All of the samples display single-step degradation processes, and the onset temperatures of thermal degradation of the composites are increased after compounding with DCP or PBS-*g*-CNC. Thermal stability parameters of composites are summarized in Table 5 ΔW is the weight-loss percentage of samples at 200 °C, and $T_{5\%}$ is the temperature corresponding to the 5% weight loss of the composites. The activation energy for thermal decomposition is calculated

Table 5
Thermal stability parameters of the PBS/PLA (30/70) composites.

DCP/PBS-*g*-CNC	ΔW^* (%)	$T_{5\%}$ (°C)	T_{max} (°C)	E_t (kJ/mol)
0/0	0.44	355	366	90
0/2.0	0.42	355	379	86
0.2/0	0.51	357	384	97
0.2/2.0	0.47	358	385	102

* ΔW is the weight-loss percentage of samples at 200 °C.

from the TGA curves by the integral method proposed by Horowitz and Metzger with the following equation (Chen & Yoon, 2005):

$$\ln\left\{ln\left[\frac{1}{1-\alpha}\right]\right\} = \frac{E_t\theta}{RT_{max}^2} \quad (1)$$

where α is the decomposed fraction of the sample, E_t is the activation energy for decomposition, T_{max} is the temperature at the maximum rate of weight loss, θ is $T-T_{max}$ (where T is the temperature), and R is the gas constant. E_t is calculated from the slope of the straight line of $\ln\{\ln[1/(1-\alpha)]\}$ *versus* θ and summarized in Table 5.

W_{200} value of PBS/PLA blend has little change in compositions. The composites modified with DCP exhibit slightly higher $T_{5\%}$, T_{max} and E_t than PBS/PLA, and the values are increased by the addition of 2.0 phr PBS-*g*-CNC. This reveals that the thermal stability of the PBS/PLA blend is improved by the addition of DCP. This could be attributed to the formation of crosslink structure, which reduces the chains mobility and inhibits the chain unzipping during the propagation of the degradation process (Ahmad & Luyt, 2012). The composite with 2.0 phr PBS-*g*-CNC displays lower E_t than PBS/PLA, which could be owing to the lower thermal stability of CNC (Roman & Winter, 2004).

4. Conclusions

A novel bio-based filler PBS-*g*-CNC has been successfully *in situ* synthesized and its structure was confirmed by FTIR, ^{13}C NMR, XPS and GPC analysis after saponification. PBS-*g*-CNC could be used to reinforce PBS/PLA (30/70) blend with DCP as a compatibilizer. Both DCP and PBS-*g*-CNC show great effects on the morphology, crystallization behavior and mechanical properties of PBS/PLA composites.

The average size of PBS droplets in PLA continuous phase of the PBS/PLA blend can be decreased by adding either 0.2 phr DCP or 2.0 phr PBS-*g*-CNC. For the PBS/PLA/PBS-*g*-CNC (30/70/2.0) composites with and without 0.2 phr DCP, PBS-*g*-CNC is dispersed in both PBS

and PLA phases, which contributes to improve the crystallization and mechanical properties of the composites.

As confirmed by WAXD results, the crystallinity of PBS/PLA composites is increased from 12% to 30% with increasing PBS-*g*-CNC content from 0 to 2.0 phr. Among crystals in composites, α′-phase crystal of PLA is more sensitive to the addition of PBS-*g*-CNC than PBS crystals, which can be revealed by an obvious increase of α′-phase crystal peaks. The crystallinity of both PBS and PLA components is decreased by the addition of 0.2 phr DCP.

The mechanical and dynamical mechanical properties and thermal stability of PBS/PLA blend are significantly improved by adding DCP and PBS-*g*-CNC. With increasing PBS-*g*-CNC content from 0 to 2.0 phr the impact strength of PBS/PLA blend with 0.2 phr DCP increases from 105 to 726 J/m. At a given temperature below 48 °C, PBS/PLA/DCP/PBS-*g*-CNC (30/70/0.2/2.0) composite shows highest storage modulus and glass transition temperature in all the PBS/PLA composites.

Acknowledgement

The authors gratefully acknowledge National Natural Science Foundation of China (Nos. 51273109 and 51235008) for the financial support.

References

Ahmad, E. E. M., & Luyt, A. S. (2012). Morphology, thermal, and dynamic mechanical properties of poly(lactic acid)/sisal whisker nanocomposites. *Polymer Composites*, *33*, 1025–1032.

Ahn, B. D., Kim, S. H., Kim, Y. H., & Yang, J. S. (2001). Synthesis and characterization of the biodegradable copolymers from succinic acid and adipic acid with 1,4-butanediol. *Journal of Applied Polymer Science*, *82*, 2808–2826.

Anderson, K. S., Schreck, K. M., & Hillmyer, M. A. (2008). Toughening polylactide. *Polymer Reviews*, *48*, 85–108.

Arrieta, M., Fortunati, E., Dominici, F., López, J., & Kenny, J. M. (2015). Bionanocomposite films based on plasticized PLA–PHB/cellulose nanocrystal blends. *Carbohydrate Polymers*, *121*, 265–275.

Cao, X. D., Habibi, Y., & Lucia, L. A. (2009). One-pot polymerization, surface grafting, and processing of waterborne polyurethane–cellulose nanocrystal nanocomposites. *Journal of Materials Chemistry*, *19*, 7137–7145.

Cherykhunthod, W., Seadan, M., & Suttiruengwong, S. (2015). Effect of peroxide and chain extender on mechanical properties and morphology of poly(butylene succinate)/poly(lactic acid) blends. In *Proceedings of the IOP Conference Series: Materials Science and Engineering* (pp. 1–7). IOP Publishing.

Chen, G. X., & Yoon, J. S. (2005). Thermal stability of poly(L-lactide)/poly(butylene succinate)/clay nanocomposites. *Polymer Degradation and Stability*, *88*, 206–212.

Guo, T., Ding, X., Han, H., Zhang, L., Zhang, Y., & Zhou, K. (2012). Wide-angle X-ray diffraction investigation on crystallization behavior of PA6/PS/SEBS-*g*-MA blends. *Journal of Polymer Research*, *19*, 1–5.

Harada, M., Ohya, T., Iida, K., Hayashi, H., Hirano, K., & Fukuda, H. (2007). Increased impact strength of biodegradable poly(lactic acid)/poly(butylene succinate) blend composites by using isocyanate as a reactive processing agent. *Journal of Applied Polymer Science*, *106*, 1813–1820.

Jiang, L., Wolcott, M. P., & Zhang, J. (2006). Study of biodegradable polylactide/poly(butylene adipate-*co*-terephthalate) blends. *Biomacromolecules*, *7*, 199–207.

Ji, D., Liu, Z., Lan, X., Wu, F., Xie, B., & Yang, M. (2014). Morphology, rheology, crystallization behavior, and mechanical properties of poly(lactic acid)/poly(butylene succinate)/dicumyl peroxide reactive blends. *Journal of Applied Polymer Science*, *131*, 39580.

Kargarzadeh, H., Sheltami, R. M., Ahmad, I., Abdullah, I., & Dufresne, A. (2015). Cellulose nanocrystal: A promising toughening agent for unsaturated polyester nanocomposite. *Polymer*, *56*, 346–357.

Kawai, T., Rahman, N., Matsuba, G., Nishida, K., Kanaya, T., Nakano, M., et al. (2007). Crystallization and melting behavior of poly(L-lactic acid). *Macromolecules*, *40*, 9463–9469.

Lin, N., & Dufresne, A. (2013). Supramolecular hydrogels from in situ host–guest inclusion between chemically modified cellulose nanocrystals and cyclodextrin. *Biomacromolecules*, *14*, 871–880.

Lin, N., Huang, J., Chang, P. R., Feng, J., & Yu, J. (2011). Surface acetylation of cellulose nanocrystal and its reinforcing function in poly(lactic acid). *Carbohydrate Polymers*, *83*, 1834–1842.

Lin, N., Yu, J. H., Chang, P. R., Li, J. L., & Huang, J. (2011). Poly(butylene succinate)-based biocomposites filled with polysaccharide nanocrystals: Structure and properties. *Polymer Composites*, *32*, 472–482.

Lin, S., Huang, J., Chang, P. R., Wei, S., Xu, Y., & Zhang, Q. (2013). Structure and mechanical properties of new biomass-based nanocomposite: Castor oil-based polyurethane reinforced with acetylated cellulose nanocrystal. *Carbohydrate Polymers*, *95*, 91–99.

Lizundia, E., Vilas, J. L., & León, L. M. (2015). Crystallization, structural relaxation and thermal degradation in poly(L-lactide)/cellulose nanocrystal renewable nanocomposites. *Carbohydrate Polymers*, *123*, 256–265.

Ludvik, C. N., Glenn, G. M., Klamczynski, A. P., & Wood, D. F. (2007). Cellulose fiber/bentonite clay/biodegradable thermoplastic composites. *Journal of Polymers and the Environment*, *15*, 251–257.

Ma, P., Cai, X., Zhang, Y., Wang, S., Dong, W., Chen, M., et al. (2014). *In situ* compatibilization of poly(lactic acid) and poly(butylene adipate-*co*-terephthalate) blends by using dicumyl peroxide as a free-radical initiator. *Polymer Degradation and Stability*, *102*, 145–151.

Nagarajan, V., Zhang, K., Misra, M., & Mohanty, A. K. (2015). Overcoming the fundamental challenges in improving the impact strength and crystallinity of PLA biocomposites: Influence of nucleating agent and mold temperature. *ACS Applied Materials & Interfaces*, *7*, 11203–11214.

Nerkar, M., Ramsay, J. A., Ramsay, B. A., Vasileiou, A. A., & Kontopoulou, M. (2015). Improvements in the melt and solid-state properties of poly(lactic acid), poly-3-hydroxyoctanoate and their blends through reactive modification. *Polymer*, *64*, 51–61.

Rasal, R. M., Janorkar, A. V., & Hirt, D. E. (2010). Poly(lactic acid) modifications. *Progress in Polymer Science*, *35*, 338–356.

Roman, M., & Winter, W. T. (2004). Effect of sulfate groups from sulfuric acid hydrolysis on the thermal degradation behavior of bacterial cellulose. *Biomacromolecules*, *5*, 1671–1677.

Rueda, L., Saralegi, A., Fernández-d'Arlas, B., Zhou, Q., Alonso-Varona, A., Berglund, L. A., et al. (2013). *In situ* polymerization and characterization of elastomeric polyurethane–cellulose nanocrystal nanocomposites. Cell response evaluation. *Cellulose*, *20*, 1819–1828.

Shang, W. L., Huang, J., Luo, H., Chang, P. R., Feng, J. W., & Xie, G. Y. (2013). Hydrophobic modification of cellulose nanocrystal via covalently grafting of castor oil. *Cellulose*, *20*, 179–190.

Shibata, M., Inoue, Y., & Miyoshi, M. (2006). Mechanical properties, morphology, and crystallization behavior of blends of poly(L-lactide) with poly(butylene succinate-*co*-L-lactate) and poly(butylene succinate). *Polymer*, *47*, 3557–3564.

Shibata, M., Teramoto, N., & Inoue, Y. (2007). Mechanical properties, morphologies, and crystallization behavior of plasticized poly(L-lactide)/poly(butylene succinate-*co*-L-lactate) blends. *Polymer*, *48*, 2768–2777.

Signori, F., Boggioni, A., Righetti, M. C., Rondán, C. E., Bronco, S., & Ciardelli, F. (2015). Evidences of transesterification, chain branching and cross-linking in a biopolyester commercial blend upon reaction with dicumyl peroxide in the melt. *Macromolecular Materials and Engineering*, *300*, 153–160.

Wang, R., Wang, S., & Zhang, Y. (2009). Morphology, rheological behavior, and thermal stability of PLA/PBSA/POSS composites. *Journal of Applied Polymer Science*, *113*, 3095–3102.

Wang, R., Wang, S., Zhang, Y., Wan, C., & Ma, P. (2009). Toughening modification of PLLA/PBS blends via in situ compatibilization. *Polymer Engineering and Science*, *49*, 26–33.

Wu, D., Yuan, L., Laredo, E., Zhang, M., & Zhou, W. (2012). Interfacial properties, viscoelasticity, and thermal behaviors of poly(butylene succinate)/polylactide blend. *Industrial & Engineering Chemistry Research*, *51*, 2290–2298.

Xu, L. Q., & Huang, H. X. (2012). Relaxation behavior of poly(lactic acid)/poly(butylene succinate) blend and a new method for calculating its interfacial tension. *Journal of Applied Polymer Science*, *125*, E272–E277.

Xu, S., Girouard, N., Schueneman, G., Shofner, M. L., & Meredith, J. C. (2013). Mechanical and thermal properties of waterborne epoxy composites containing cellulose nanocrystals. *Polymer*, *54*, 6589–6598.

Yasuniwa, M., Sakamo, K., Ono, Y., & Kawahara, W. (2008). Melting behavior of poly(L-lactic acid): X-ray and DSC analyses of the melting process. *Polymer*, *49*, 1943–1951.

Zeng, J., Li, K., & Du, A. (2015). Compatibilization strategies in poly(lactic acid)-based blends. *RSC Advances*, *5*, 32546–32565.

Zhang, K., Mohanty, A. K., & Misra, M. (2012). Fully biodegradable and biorenewable ternary blends from polylactide, poly(3-hydroxybutyrate-*co*-hydroxyvalerate) and poly(butylene succinate) with balanced properties. *ACS Applied Materials & Interfaces*, *4*, 3091–3101.

Zhang, X., & Zhang, Y. (2015). Poly(butylene succinate-*co*-butylene adipate)/cellulose nanocrystal composites modified with phthalic anhydride. *Carbohydrate Polymers*, *134*, 52–59.

Zheng, L., Li, C., Zhang, D., Guan, G., Xiao, Y., & Wang, D. (2011). Synthesis, characterization and properties of novel biodegradable multiblock copolymers comprising poly(butylene succinate) and poly(1,2-propylene terephthalate) with hexamethylene diisocyanate as a chain extender. *Polymer International*, *60*, 666–675.